JOC The Journal of Organic Chemistry

Featured Article

pubs.acs.org/joc

Fungal Biotransformation of Tetracycline Antibiotics

Zhuo Shang,[†] Angela A. Salim,[†] Zeinab Khalil,[†] Paul V. Bernhardt,[‡] and Robert J. Capon*[,†]

[†]Institute for Molecular Bioscience and [‡]School of Chemistry and Molecular Biosciences, The University of Queensland, St. Lucia, QLD 4072, Australia

Supporting Information

ABSTRACT: The commercial antibiotics tetracycline (**3**), minocycline (**4**), chlortetracycline (**5**), oxytetracycline (**6**), and doxycycline (**7**) were biotransformed by a marine-derived fungus *Paecilomyces* sp. to yield *seco*-cyclines A–H (**9**–**14**, **18** and **19**) and *hemi*-cyclines A–E (**20**–**24**). Structures were assigned by detailed spectroscopic analysis, and in the case of **10** X-ray crystallography. Parallel mechanisms account for substrate-product specificity, where **3**–**5** yield *seco*-cyclines and **6** and **7** yield *hemi*-cyclines. The susceptibility of **3**–**7** to fungal biotransformation is indicative of an unexpected potential for tetracycline "degradation" (i.e., antibiotic resistance) in fungal genomes. Significantly, the fungal-derived tetracycline-like viridicatumtoxins are resistant to fungal biotransformation, providing chemical insights that could inform the development of new tetracycline antibiotics resistant to enzymatic degradation.

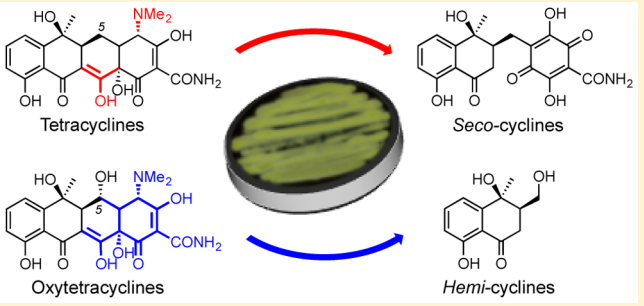

INTRODUCTION

We recently reported on a rare class of tetracycline-like polyketide (i.e., viridicatumtoxin A (**1**)) produced by an Australian marine mollusk-associated fungus, *Paecilomyces* sp. (CMB-MF010).[1] In the course of those studies, we noted that the minor 5-oxocometabolite, viridicatumtoxin B (**2**), was exceptionally potent against vancomycin-resistant *Enterococci* (VRE) (MIC 40 nM). Unfortunately, further in vivo antibiotic investigations stalled due to low fermentation yields. While an elegant total synthesis of (±)-**2** had been reported,[2,3] we elected to investigate the anti-VRE properties of the viridicatumtoxin pharmacophore by transforming commercially available tetracycline (**3**), minocycline (**4**), chlortetracycline (**5**), oxytetracycline (**6**), and doxycycline (**7**) (Figure 1). More specifically, we hypothesized that 5-oxotetracyclines may exhibit enhanced anti-VRE properties, akin to those observed in the structure–activity relationship between **1** and **2**.

While the chemical oxidation of **7** to the 5-oxodoxycycline (**8**) had been noted (albeit not well documented),[4] in our hands this transformation was not reproducible. Drawing inspiration from the ability of CMB-MF010 to biosynthesize the cometabolites **1** and **2**, we set out to investigate whether CMB-MF010 could mediate the oxidative biotransformation of **3**–**7** to yield 5-oxotetracyclines as potential antibiotic surrogates of viridicatumtoxin B (**2**).

Curiously, despite reports on the fungal biotransformation of fluoroquinolone antibiotics (e.g., flumequine,[5] danofloxacin,[6] norfloxacin,[7] and ciprofloxacin[7]), to the best of our knowledge there are no accounts of the biotransformation of tetracyclines by a defined filamentous fungus. This is a surprising knowledge gap, especially as tetracyclines are well-known contaminants in urban, rural, and industrial waste where they can drive antibiotic resistance in pathogens and potentially compromise microbiological processes that underpin waste management. These same environments are rich in fungal biodiversity.

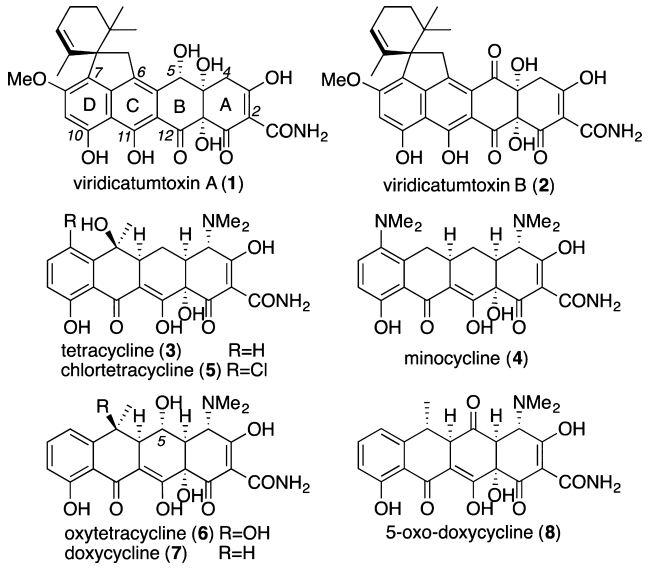

Figure 1. Examples of known viridicatumtoxins and tetracyclines.

RESULTS AND DISCUSSION

To develop methodology for the biotransformation of tetracyclines by *Paecilomyces* sp. (CMB-MF010), we carried out preliminary analytical-scale 30-day PYG agar and broth cultivations. As our commercial sample of tetracycline (**3**) was

Received: May 27, 2016
Published: July 15, 2016

DOI: 10.1021/acs.joc.6b01272
J. Org. Chem. 2016, 81, 6186–6194

contaminated with ~10% 4-*epi*-tetracycline (**3a**), likely generated by autocatalytic acid mediated keto−enol tautomerism[8] (Figure 2), biotransformation trials were performed on

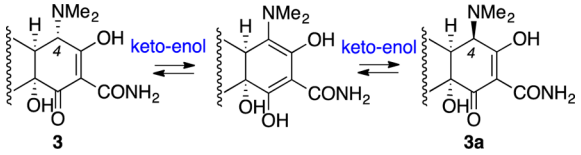

Figure 2. Acid-mediated equilibration of **3** and **3a**.

this mixture. Of note, conversion of **3** to **3a** was enhanced 3-fold to ~30% when cultivated in media without inoculation (negative control), consistent with an autocatalytic interconversion. CMB-MF010-inoculated PYG agar cultivations of **3**/**3a** revealed quantitative conversion to **9**−**11**, while PYG broth cultivations exhibited modest conversion to **9** and **12**. By contrast, PYG agar and broth cultivations on oxytetracycline (**6**) resulted in quantitative conversion to a single major product **20**, and trace levels of **21**. On the basis of these trials, multiple preparative-scale biotransformation studies were performed using 30-day PYG single agar plate cultivations of CMB-MF010, each loaded with the HCl salt of a commercial tetracycline antibiotic (40 mg). All biotransformation products were isolated by HPLC, and the structures were assigned by detailed spectroscopic analysis.

A 30-day agar plate cultivation of CMB-MF010 treated with **3**:**3a** (9:1) afforded >95% biotransformation to *seco*-cyclines A−C (**9**−**11**) (Figure S1). HRESI(+)MS analysis of **9** returned a quasimolecular ion consistent with a molecular formula ($C_{19}H_{17}NO_8$, Δmmu −0.1) having lost the elements of CH and $N(CH_3)_2$. Comparison of 1D NMR (DMSO-d_6) data (Tables 1 and 2) for **9** with **3** suggested conservation of rings C and D, loss of the ring A 4-$N(CH_3)_2$ with oxidation to a fully substituted *p*-quinone, and opening of ring B across C-11a to C-12a with associated loss of C-12. Diagnostic 2D NMR correlations (Figure 3) supported the assignment of the structure for *seco*-cycline A (**9**) as shown, with retention of the C-5a and C-6 configuration (evident in **3**) validated by comparison to the cobiotransformation product **10**.

Table 1. ^{1}H NMR (600 MHz, DMSO-d_6) Data for *seco*-Cyclines A−D (9−12)

position	*seco*-cycline A (**9**)	*seco*-cycline B (**10**)	*seco*-cycline C (**11**)	*seco*-cycline D (**12**)
5	α 2.76 (m)[a]	α 2.75 (dd, 12.9, 3.6)	α 2.64 (dd, 17.8, 6.0)[b]	α 2.76 (dd, 13.2, 4.3)
	β 2.17 (dd, 13.0, 12.1)	β 2.14 (dd, 12.9, 11.7)	β 1.85 (dd, 17.8, 8.3)[c]	β 2.51 (dd, 13.2, 11.6)
5a	2.36 (m)	2.36 (m)	2.62 (m)[b]	3.17 (dd, 11.6, 4.3)
7	7.20 (dd, 7.8, 0.9)	7.20 (d, 7.7)	6.99 (d, 6.8)	7.21 (d, 7.6)
8	7.57 (dd, 8.3, 7.8)	7.56 (dd, 8.3, 7.7)	7.60 (dd, 8.2, 6.8)	7.66 (dd, 8.6, 7.6)
9	6.83 (dd, 8.3, 0.9)	6.83 (d, 8.3)	6.94 (d, 8.2)	7.09 (d, 8.6)
11a	α 2.76 (m)[a]	α 2.78 (dd, 18.5, 5.0)	α 3.27 (br d, 18.6)	3.50 (br s)
	β 2.45 (dd, 18.8, 4.5)	β 2.45 (dd, 18.5, 4.4)	β 2.82 (dd, 18.6, 3.0)	
6-CH_3	1.54 (s)	1.54 (s)	1.81 (s)[c]	1.93 (s)
1-NH_2		α 10.80 (d, 4.5)		
		β 8.91 (d, 4.5)		
2-$CONH_2$	α 9.43 (br s)	α 8.49 (d, 3.4)	α 9.46 (br s)	α 9.43 (br s)
	β 9.13 (br s)	β 7.39 (d, 3.4)	β 9.24 (br s)	β 9.16 (br s)
10-OH	12.6 (s)	12.6 (s)	12.4 (s)	11.4 (s)

[a−c]Overlapping signals with assignments supported by HSQC correlations.

Table 2. ^{13}C NMR (150 MHz, DMSO-d_6) Data for *seco*-Cyclines A−D (9−12)

position	**9**	**10**	**11**	**12**
1	nd[a]	155.6	175.0	nd
2	98.0	95.8	98.7	98.2
3	nd	177.2	178.7	177.9
4	nd	158.9	153.9	nd
4a	118.3	114.8	117.3	115.1
5	22.0	21.9	22.0	21.5
5a	43.3	43.3	34.1	52.5
6	71.0	71.1	79.3	86.7
6a	150.8	150.8	145.8	144.4
7	116.4	116.4	115.5	115.5
8	137.0	137.0	138.0	137.8
9	115.6	115.6	117.5	119.7
10	161.3	161.3	161.8	162.0
10a	114.6	114.6	114.0	112.6
11	203.9	203.9	202.3	194.7
11a	39.0	39.1	40.3	62.1
12				170.6
12a	nd	180.0	179.3	nd
2-$CONH_2$	172.1	169.3	172.4	172.1
6-CH_3	30.2	30.3	27.9	16.8

[a]nd: undetected carbon signals due to tautomerization.

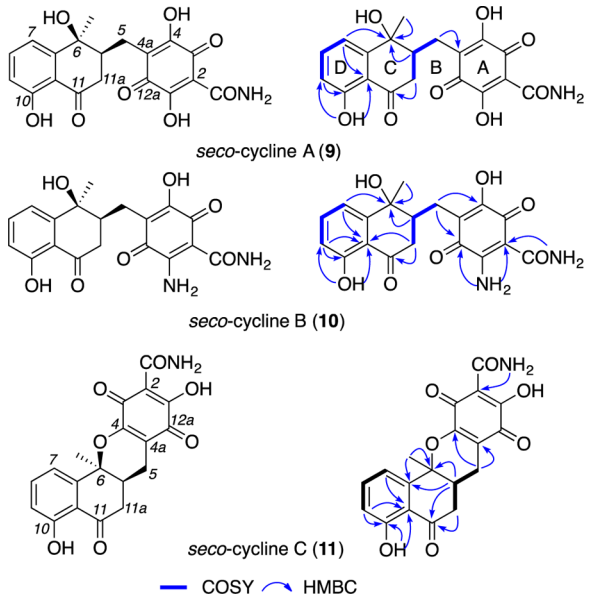

Figure 3. Structures and diagnostic 2D NMR correlations for **9**−**11**.

HRESI(+)MS analysis of **10** revealed a quasimolecular ion consistent with a molecular formula ($C_{19}H_{18}N_2O_7$, Δmmu −0.2) for an NH_2 substitution analogue of **9**. Comparison of 1D NMR (DMSO-d_6) data (Tables 1 and 2) for **10** with **9**

DOI: 10.1021/acs.joc.6b01272
J. Org. Chem. 2016, 81, 6186−6194

revealed the only significant difference as the appearance of an amine moiety (δ_H 10.80 and 8.91), which diagnostic 2D NMR correlations positioned at C-1 (Figure 3). These considerations, together with X-ray crystallographic analysis (Figure 4), supported the structure for *seco*-cycline B (**10**) as shown. Significantly, as noted above for **9**, the C-5a and C-6 configuration in **10** was retained from **3**.

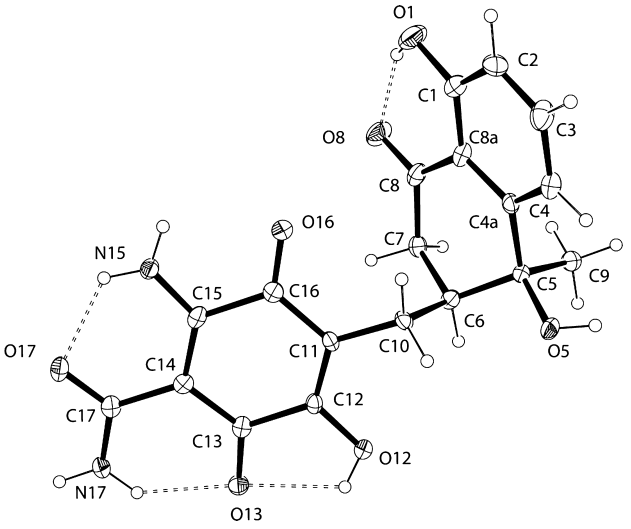

Figure 4. ORTEP structure generated from the single-crystal X-ray diffraction of **10** showing 30% probability ellipsoids. (Note: different numbering systems are used for the structures in the text.)

HRESI(+)MS analysis of **11** exhibited a quasimolecular ion consistent with a molecular formula ($C_{19}H_{15}NO_7$, Δmmu +0.6) for a dehydrated analogue of **9**. Comparison of the 1D NMR (DMSO-d_6) data (Tables 1 and 2) for **11** with **9** revealed a downfield shift of C-6 ($\Delta\delta_C$ +8.3) and an upfield shift for C-5a ($\Delta\delta_C$ −9.2), C-6a ($\Delta\delta_C$ −5.0), and 6-CH_3 ($\Delta\delta_C$ −2.3), consistent with the changes to the C-6 substitution. Diagnostic 2D NMR correlations (Figure 3), together with a facile acid-mediated conversion of **9** to **11**, supported assignment of the structure for *seco*-cycline C (**11**) as shown, with the C-5a and C-6 absolute configuration retained from **3**.

Exposure of **3**:**3a** (9:1) to a shorter duration 15-day agar plate cultivation of CMB-MF010 yielded the additional minor biotransformation product *seco*-cycline D (**12**) (Figure S1). HRESI(+)MS analysis of **12** returned a quasimolecular ion consistent with a molecular formula ($C_{20}H_{15}NO_9$, Δmmu +0.7) for a + CO_2 homologue of **11**. Comparison of the 1D NMR (DMSO-d_6) data (Tables 1 and 2) for **12** with **11** revealed conversion of the C-11a methylene to a methine and the appearance of a new ester/lactone carbonyl resonance. These considerations, together with diagnostic 2D NMR correlations (Figure 5), supported the structure assigned to *seco*-cycline D

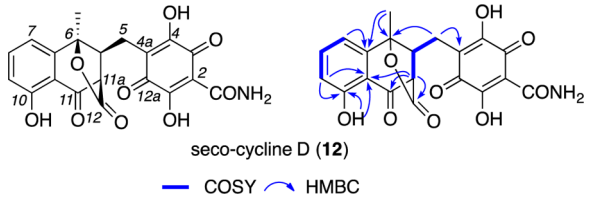

Figure 5. Structure and diagnostic 2D NMR correlations for **12**.

(**12**) as shown, with the C-5a and C-6 configuration retained from **3**, and the C-11a configuration defined by a stereospecific *β*-facial lactonisation. Of note, **12** was cited (but not fully characterized) in two 1969 patents documenting the biotransformation of **3** by plant and fungi peroxidases and by oxidation with *m*-chloroperbenzoic acid.[9,10]

Minocycline (**4**) underwent quantitative biotransformation when exposed to a 30-day agar plate cultivation of CMB-MF010, yielding *seco*-cyclines E and F (**13** and **14**) (Figure S2). HRESI(+)MS analysis of **13** and **14** revealed quasimolecular ions corresponding to molecular formula $C_{20}H_{20}N_2O_7$ (Δmmu −0.4) and $C_{20}H_{21}N_3O_6$ (Δmmu −0.4), respectively. Analysis of 1D NMR (DMSO-d_6) data (Table 3) suggested the biotransformation products akin to **9** and **10** derived from **3**:**3a**. These considerations, together with diagnostic 2D NMR correlations (Figure 6), supported assignment of structures for *seco*-cyclines E (**13**) and F (**14**) as shown, with retention of the C-5a configuration from **4**. Of note, a 2010 report described the Ag_2CO_3/EDTA (66% yield) and $Hg(OAc)_2$ (88% yield) preparation of 4,11a-bridged derivatives of **4**, which were readily converted to **13** (55% yield) via decarboxylative rearrangement in acidic aqueous phosphate buffer (pH 6.4) at 35 °C.[11]

Our commercial sample of **5** was contaminated with three isomers tentatively identified on the basis of HRESI(+)MS as 4-*epi*-chlortetracycline (**15**) ($C_{22}H_{23}ClN_2O_8$, Δmmu +0.3), isochlorotetracycline (**16**) ($C_{22}H_{23}ClN_2O_8$, Δmmu −0.3), and 4-*epi*-isochlortetracycline (**17**) ($C_{22}H_{23}ClN_2O_8$, Δmmu −0.4) (Figure 7).[12,13] The acid-mediated epimerization of **5** to **15** likely proceeds as illustrated above for **3**:**3a** (Figure 2) with the ring D Cl substituent further activating the C-11 carbonyl to intramolecular lactonization and cleavage of C-11 to C-11a to yield **16** and **17** (Figure 8). Of note, the conversion of **5** to **15**−**17** was enhanced during cultivation without CMB-MF010 inoculation (negative control) (Figure S3). Notwithstanding chemical stability considerations, CMB-MF010 did biotransform **5** to *seco*-cyclines A (**9**) and B (**10**) (Figure S3), which were identified by HRESIMS and HPLC coelution with authentic standards (prepared from **3**). Furthermore, on the basis of HRESIMS and mechanistic considerations (Figure 11), we detected the presence of chloro analogues tentatively identified as *seco*-cyclines G (**18**) ($C_{19}H_{16}ClNO_8$, Δmmu +0.1) and H (**19**) ($C_{19}H_{17}ClN_2O_7$, Δmmu +0.1) (Figure 7 and Table S1).

Oxytetracycline (**6**) underwent quantitative biotransformation when exposed to 30-day agar plate cultivations of CMB-MF010, yielding *hemi*-cyclines A−B (**20** and **21**) (Figure S4). HRESI(−)MS analysis of **20** returned a quasimolecular ion consistent with a molecular formula ($C_{12}H_{14}O_4$, Δmmu −0.5) suggestive of a substituted ring C/D tetralone. Analysis of the NMR (CD_3OD) data (Table 4), and in particular diagnostic 2D NMR correlations (Figure 9), supported assignment of the structure for *hemi*-cycline A (**20**) as shown, with the C-6 configuration retained from **6**. The C-5a configuration in **20** was assigned by comparison of $J_{11a\alpha,5a}$ and $J_{11a\beta,5a}$ measurements with **20a** (Figure 9), a C-5a epimer produced by *Streptomyces rimosus* (R1059), a mutant strain used in the commercial production of **6**.[14] HRESI(+)MS analysis of **21** returned a quasimolecular ion consistent with a molecular formula ($C_{14}H_{16}O_5$, Δmmu +0.1) for an acetate derivative of **20**. Comparison of the 1D NMR (CD_3OD) data (Table 4) for **21** with **20** revealed the only significant differences as deshielding of the C-5 methylene and the appearance of resonances for a C-

DOI: 10.1021/acs.joc.6b01272
J. Org. Chem. 2016, 81, 6186−6194

Table 3. ^{1}H and ^{13}C NMR (600 MHz, DMSO-d_6) Data for *seco*-Cyclines E and F (13 and 14)

	seco-cycline E (**13**)		*seco*-cycline F (**14**)	
position	δ_H (mult, J (Hz))	δ_C	δ_H (mult, J (Hz))	δ_C
1		nd		155.5
2		98.0		95.9
3		177.8		177.2
4		nd		158.7[f]
4a		117.3		114.0
5	2.50 (m)[a,g]	28.1	2.48 (dd, 7.0, 3.8)[g]	28.0
5a	2.29 (m)	33.2	2.28 (m)	33.3
6	α 3.18 (dd, 17.0, 4.0)	30.5	α 3.17 (dd, 16.8, 3.7)	30.6
	β 2.63 (dd, 17.0, 5.1)[b]		β 2.61 (m)[d]	
6a		138.4[c]		138.5[e]
7		138.4[c]		138.5[e]
8	7.57 (d, 8.8)	128.6	7.49 (br s)	128.6
9	6.84 (d, 8.8)	115.5	6.81 (d, 8.9)	115.2
10		159.1		158.7[f]
10a		116.3		116.4
11		205.7		205.8
11a	α 2.64 (m)[b]	43.7	α 2.63 (m)[d]	43.9
	β 2.53 (m)[a,g]		β 2.53 (m)[g]	
12a		nd		180.2
2-$CONH_2$		172.1		169.3
7-$N(CH_3)_2$	2.74 (br s)	45.0	2.67 (br s)[d]	44.8
1-NH_2			α 10.84 (d, 5.5)	
			β 8.94 (d, 5.5)	
2-$CONH_2$	α 9.49 (br s)		α 8.50 (d, 3.8)	
	β 9.15 (br s)		β 7.43 (d, 3.8)	
10-OH	12.36 (br s)		12.30 (br s)	

[a−f]Overlapping signals with assignments supported by HSQC and HMBC correlations. [g]Overlap with residual DMSO signal. nd: undetected carbon signals due to tautomerization.

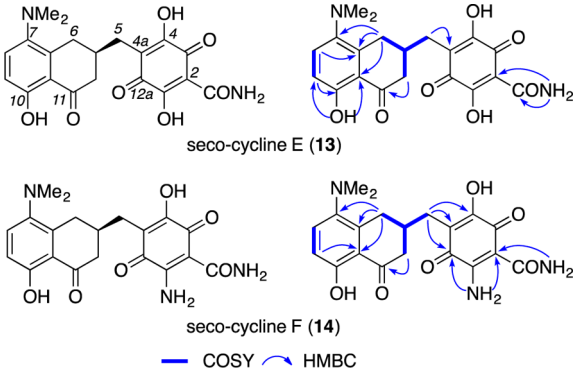

Figure 6. Structures and diagnostic 2D NMR correlations for **13** and **14**.

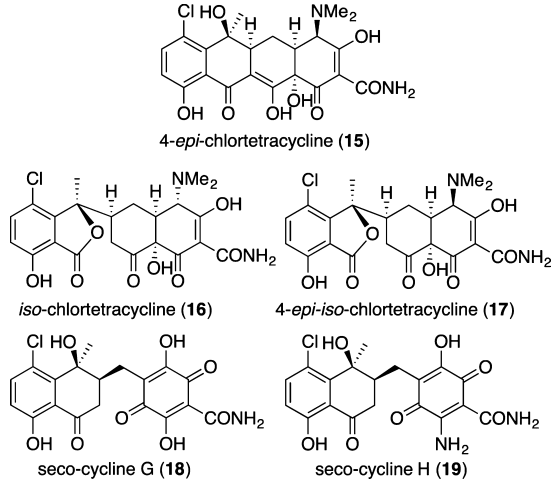

Figure 7. Degradation products **15**−**17** and CMB-MF010 biotransformation products **18** and **19**, derived from **5**.

5 acetate moiety (δ_C 20.5, $OCOCH_3$; δ_C 172.7, $OCOCH_3$). These considerations, together with diagnostic 2D NMR correlations, and $J_{11a\alpha,5a}$ and $J_{11a\beta,5a}$ measurements, permitted assignment of the structure for *hemi*-cycline B (**21**) as shown (Figure 9).

Doxycycline (**7**) underwent ∼90% biotransformation when exposed to 30-day agar plate cultivations of CMB-MF010, yielding *hemi*-cyclines C−E (**22**−**24**) (Figure S5). HRESI(+)-MS analysis of **22** returned a quasimolecular ion consistent with a molecular formula ($C_{12}H_{14}O_3$, Δmmu −0.5) for a deoxy analogue of **20**. Analysis of NMR (CD_3OD) data (Table 5), and in particular diagnostic 2D NMR correlations, and $J_{11a\alpha,5a}$ and $J_{11a\beta,5a}$ measurements, permitted assignment of the structure for *hemi*-cycline C (**22**) as shown (Figure 10), with the C-6 configuration retained from **7**. HRESI(+)MS analysis of **23** returned a quasimolecular ion consistent with a molecular formula ($C_{12}H_{12}O_4$, Δmmu −0.7) for an oxidized analogue of **22**. Comparison of the 1D NMR (CD_3OD) data (Table 5) for **23** with **22** revealed the absence of resonances for a C-5 methylene and appearance of resonances for a C-5 carboxylic acid (δ_C 177.0). These considerations, together with diagnostic HMBC correlations, and $J_{11a\alpha,5a}$ and $J_{11a\beta,5a}$ measurements, permitted assignment of the structure for *hemi*-cycline D (**23**) as shown (Figure 10), with the C-6 configuration retained from

DOI: 10.1021/acs.joc.6b01272
J. Org. Chem. 2016, 81, 6186−6194

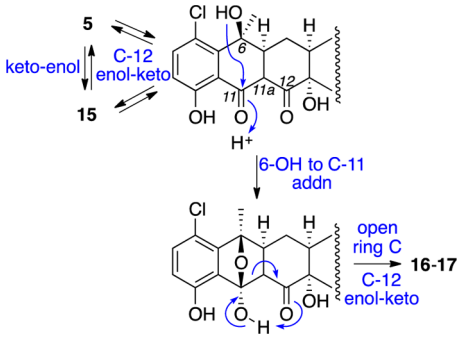

Figure 8. Mechanism for degradation of **5** to **15**–**17**.

Table 4. ^{1}H and ^{13}C NMR (600 MHz, CD_3OD) data for *hemi*-Cyclines A and B (20 and 21)

	hemi-cycline A (**20**)		*hemi*-cycline B (**21**)	
position	δ_H (mult, J (Hz))	δ_C	δ_H (mult, J (Hz))	δ_C
5	α 3.89 (dd, 11.1, 5.8)	62.9	α 4.40 (dd, 11.4, 4.2)	65.0
	β 3.45 (dd, 11.1, 8.0)		β 4.08 (dd, 11.4, 7.9)	
5a	2.38 (m)	48.1	2.54 (m)	46.3
6		72.8		71.6
6a		151.2		151.1
7	7.18 (dd, 7.7, 1.0)	117.1	7.17 (dd, 7.7, 1.0)	117.0
8	7.52 (dd, 8.4, 7.7)	138.2	7.52 (dd, 8.4, 7.7)	138.2
9	6.82 (dd, 8.4, 1.0)	117.3	6.83 (dd, 8.4, 1.0)	117.3
10		163.3		163.2
10a		116.1		116.3
11		205.0		204.5
11a	α 2.96 (dd, 18.6, 5.4)	39.1	α 3.03 (dd, 18.4, 5.4)	39.4
	β 2.89 (dd, 18.6, 4.3)		β 2.84 (dd, 18.4, 4.0)	
6-CH_3	1.62 (s)	31.3	1.64 (s)	31.4
5-O$COCH_3$				172.7
5-OCOCH_3			1.88 (s)	20.5

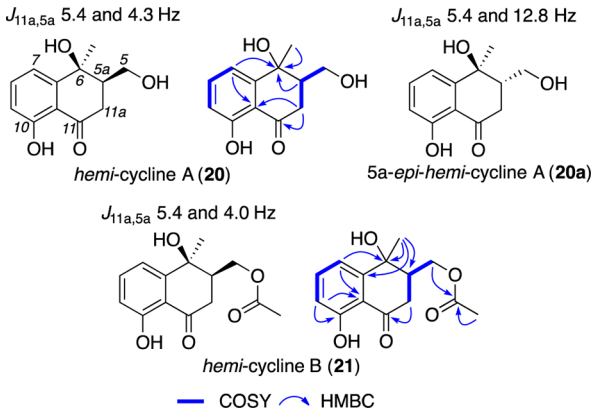

Figure 9. Structures and diagnostic NMR data for **20**, **21**, and **20a**.

7. HRESI(+)MS analysis of **24** returned a quasimolecular ion consistent with a molecular formula ($C_{12}H_{12}O_5$, Δmmu +0.4) for an oxidized analogue of **23**. Comparison of the 1D NMR (CD_3OD) data (Table 5) for **24** with **23** revealed the absence of resonances for an aromatic methine, and the appearance of resonances for an oxygenated aromatic quaternary carbon (δ_C 145.3). These considerations, together with diagnostic 2D NMR correlations, and $J_{11a\alpha,5a}$ and $J_{11a\beta,5a}$ measurements, permitted assignment of the structure for *hemi*-cycline E (**24**) as shown (Figure 10), with the C-6 configuration retained from 7.

The results from our studies demonstrate that **3**–**5** share a common mechanism of fungal biotransformation, leading to *seco*-cyclines A–H (**9**–**14**, **18**, and **19**), whereas **6** and **7** share an alternate mechanism of fungal biotransformation, leading to *hemi*-cyclines A–E (**20**–**24**), drawing attention to a substrate-product specificity that correlates with C-5 hydroxylation. For example, as illustrated for **3**:**3a**, we propose a mechanism initiated by enol–keto tautomerism to deliver a C-12 carbonyl, which undergoes enzymatic nucleophilic addition/oxidation and subsequent opening of ring B across the C-12 to C-12a bond (Figure 11). Importantly, deamination followed by oxidation assembles the quinone ring A common to *seco*-cyclines A (**9**) and D (**12**), with regioselective addition of NH_3 via the doubly activated tetramic acid C-1, with concomitant loss of H_2O, leading to the amino quinone ring A common to *seco*-cycline B (**10**). Two alternate routes for lactonization deliver *seco*-cyclines C (**11**) and D (**12**), with configurations dictated by preexisting stereochemistry about C-6a in **11** and C-6 in **12**. Following this same mechanism, minocycline (**4**) can yield *seco*-cyclines E (**13**) and F (**14**), while chlortetracycline (**5**) can yield *seco*-cyclines G (**18**) and H (**19**). That **5** can also yield **9** and **10** is attributed to partial dechlorination to **3**. By contrast, we propose that fungal biotransformation of the C-5 hydroxylated antibiotics oxytetracycline (**6**) and doxycycline (**7**) proceeds by a closely related but different mechanism. For example, as illustrated for **6** (Figure 12), we propose a mechanism initiated by the same enol–keto tautomerism, with enzymatic nucleophilic addition/oxidation and opening of ring B about the C-12 to C-12a bond. However, rather than deamination (Figure 11), we hypothesize that ring A aromatization is achieved by an alternate elimination with the C-5 hydroxy moiety influencing cleavage of the C-4a to C-5 bond to yield *hemi*-cyclines A (**20**) and B (**21**) (Figure 12). Following this same mechanism, doxycycline (**7**) can yield *hemi*-cycline C (**22**), with further oxidations leading to *hemi*-cyclines D (**23**) and E (**24**). These two highly conserved mechanisms (Figures 11 and 12) account for all the biotransformation products encountered during our investigations and suggest a basis for predicting fungal biotransformation products for other members of the tetracycline family of antibiotics.

Although CMB-MF010 successfully biotransformed **3**–**7**, none of these products matched our target 5-oxo scaffold. We therefore elected to investigate nine other filamentous fungi and three yeast isolates (see the Experimental Section). Intriguingly, all strains tested transformed **6** to **20**, with high conversion rates (>70%, Figure S7). By contrast, **3** was far more resilient, with biotransformation limited to *Fusarium* sp. (CMB-MF017) with >95% conversion to **9**–**12**, and *Gliocladium roseum* (ACM-4596) and *Candida guillermondii* (ACM-4553), with <30% conversion to **9** and **12** (Figure S6). We also determined that CMB-MF017 could biotransform **4** and **7**, with product distributions and yields comparable to CMB-MF010. Significantly, none of the biotransformation products **9**–**14** and **20**–**24** exhibited antibacterial activity (up to 30 μM) against a panel of Gram-positive and Gram-negative bacteria (Table S2).

The tetracyclines were among the earliest of the modern era "magic bullet" antibiotics, exhibiting broad-spectrum efficacy against a wide array of infectious diseases, including anthrax,

DOI: 10.1021/acs.joc.6b01272
J. Org. Chem. 2016, 81, 6186–6194

Table 5. ^{1}H and ^{13}C NMR (600 MHz, CD_3OD) Data for *hemi*-Cyclines C–E (22–24)

	hemi-cycline C (**22**)		*hemi*-cycline D (**23**)		*hemi*-cycline E (**24**)	
position	δ_H (mult, *J* (Hz))	δ_C	δ_H (mult, *J* (Hz))	δ_C	δ_H (mult, *J* (Hz))	δ_C
5	3.50 (d, 6.8)	64.8		177.0		177.2
5a	2.16 (m)	43.6	3.04 (m)[a]	46.7	2.99 (m)[b]	47.3
6	3.10 (qd, 7.2, 3.9)	35.8	3.51 (qd, 7.2, 3.5)	37.2	3.42 (m)	36.8
6a		150.3		148.9		138.6
7	6.83 (dd, 7.5, 1.0)	120.3	6.81 (dd, 7.5, 1.0)	119.8	6.67 (dd, 8.1, 0.8)	119.2
8	7.44 (dd, 8.4, 7.5)	138.1	7.43 (dd, 8.4, 7.5)	138.0	6.99 (d, 8.1)	123.0
9	6.74 (dd, 8.4, 1.0)	116.3	6.75 (dd, 8.4, 1.0)	116.7		145.3
10		163.7		163.7		151.7
10a		116.8		116.6		116.7
11		205.6		204.4		205.1
11a	α 2.99 (dd, 18.1, 5.3)	37.9	α 3.01 (dd, 18.1, 4.9)[a]	37.1	α 2.97 (dd, 18.1, 4.8)[b]	37.3
	β 2.65 (dd, 18.1, 4.6)		β 2.91 (dd, 18.1, 3.8)		β 2.88 (dd, 18.1, 3.9)	
6-CH_3	1.41 (d, 7.2)	21.9	1.44 (d, 7.2)	22.3	1.41 (d, 7.2)	22.3

[a,b]Overlapping signals with assignments supported by HSQC correlations.

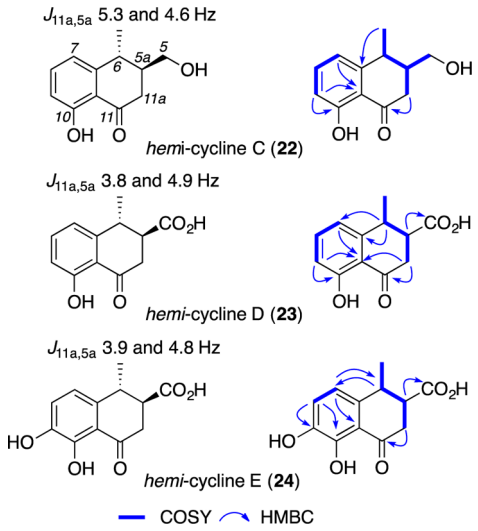

Figure 10. Structures and diagnostic NMR correlations for **22**–**24**.

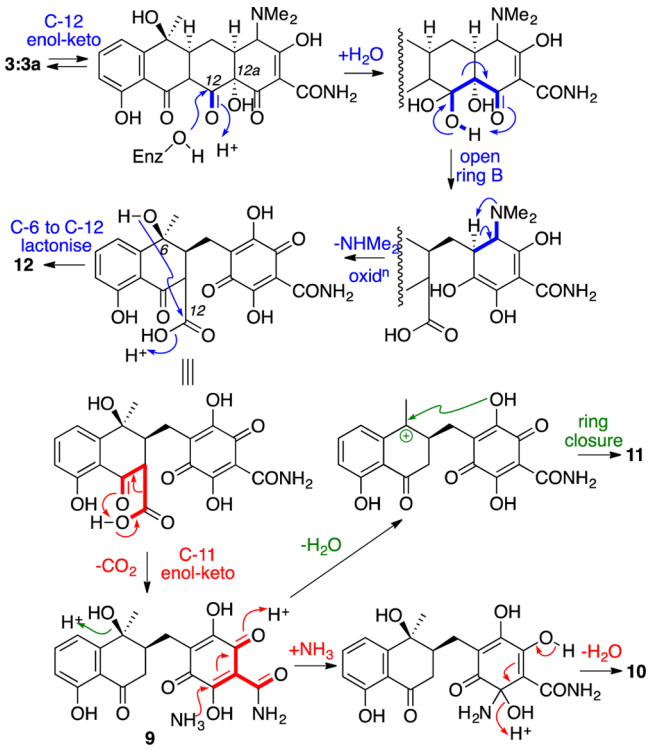

Figure 11. Mechanism for the CMB-MF010 biotransformation of **3**:**3a** to **9**–**12**.

cholera, bubonic plague, syphilis, chlamydia, and tuberculosis, as well as Lyme and Legionnaire's disease. In addition to their transformative role in human healthcare, tetracyclines played a major role in controlling disease and enhancing productivity in agriculture (e.g., livestock, aquaculture and crops).[15,16] Significantly, the continued widespread use of tetracyclines in human health and agriculture has resulted in the annual release of thousands of ton into the environment via urban sewage, rural runoff, and industrial sludge.[17] Once in the environment, tetracyclines risk being distributed via surface and groundwater, accumulating in soil and plants, entering the food chain, and exposing pathogens, as well as animals and humans, to long-term subtherapeutic antibiotic dosing. This exposure presents a very real danger of selecting for and encouraging the emergence of antibiotic resistant pathogens.[18] On the basis of our investigations, it is possible that fungi provide a hitherto unappreciated level of environmental protection, degrading tetracyclines in situ. This capability could also forewarn of a risk should fungal tetracycline degrading enzymes ever transfer to pathogens! Importantly, the *hemi*- and *seco*-cyclines could serve as biomarkers for fungi-mediated environmental degradation and the emergence of new degradative mechanisms of tetracycline resistance in pathogens.

In conclusion, although unsuccessful in our primary aim of employing fungal biotransformation to produce 5-oxo analogues of **3**–**7**, we nevertheless confirmed that these antibiotics are substrates for fungal biotransformation. When exposed to solid agar plate cultivations of the marine-derived fungi, *Paecilomyces* sp. (CMB-MF010) or *Fusarium* sp. (CMB-MF017), **3**–**5** are quantitatively transformed to *seco*-cyclines A–H (**9**–**14**, **18**, and **19**), while **6** and **7** are transformed to *hemi*-cyclines A–E (**20**–**24**), with a complete loss of antibiotic properties. We propose mechanisms that account for the observed substrate-product specificity (i.e., *seco*-cyclines versus *hemi*-cyclines) and make a comment on the possible environmental benefits and pharmaceutical and agrochemical threats posed by tetracycline-degrading fungi.

DOI: 10.1021/acs.joc.6b01272
J. Org. Chem. 2016, 81, 6186–6194

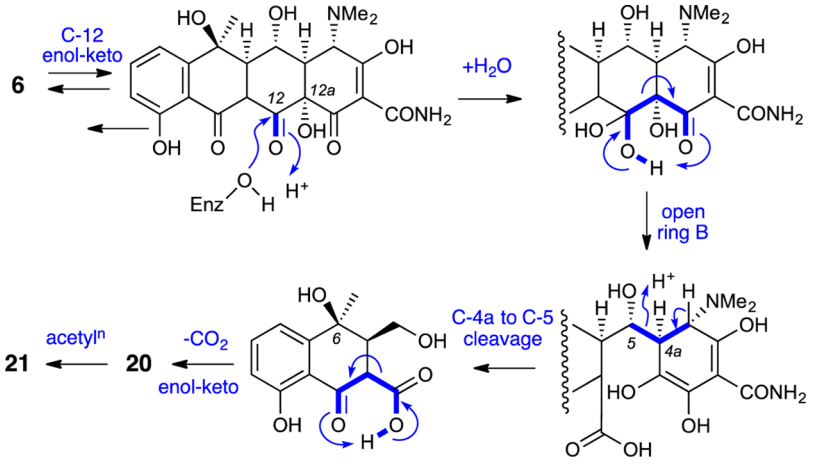

Figure 12. Mechanism for the CMB-MF010 biotransformation of **6** to **20** and **21**.

EXPERIMENTAL SECTION

Fungal Strains. Our fungal source of viridicatumtoxins, *Paecilomyces* sp. (CMB-MF010) (GenBank KT844467), was isolated from the inner tissue of a marine pulmonate false limpet *Siphonaria* sp. collected in the rocky intertidal zone, Shorncliffe, Queensland.[1] Other strains used in this study were sourced from our in-house collections, including seven marine-derived fungal isolates, *Fusarium* sp. (CMB-MF017), *Beauveria bassiana* (CMB-MF026), *Chaunopycnis* sp. (CMB-MF028), *Trichoderma hamatum* (CMB-MF030), *Penicillium roseopurpureum* (CMB-MF038), *Phomopsis* sp. (CMB-M0042F) and *Aspergillus terreus* (CMB-M0231F), two terrestrial-derived fungal isolates, *Trichoderma viride* (ACM-4595), and *Gliocladium roseum* (ACM-4596), and three yeast isolates, *Candida krusei* (ACM-4498), *Candida albicans* (ACM-4574), and *Candida guillermondii* (ACM-4553). Prior to use, all strains were recovered from cryopreservation (−80 °C in 15% aqueous glycerol).

Analysis of Solid-Phase Biotransformation of Tetracyclines 3 and 6. Solid-phase cultivation media were prepared using PYG agar (25 mL/plate, 2% glucose, 1% peptone, 0.5% yeast extract and 1.5% agar in sterile water), each treated with the HCl salt of **3** or **6** (40 mg each, prepared in 200 μL of sterile H_2O). An individual agar plate inoculated (streaked) with each of the 13 strains listed above was sealed with parafilm to prevent dehydration. These plates, including negative control plates lacking treatment of **3** and **6**, were incubated at 26.5 °C for two different time periods, 15 and 30 d, after which they were extracted with EtOAc (2 × 50 mL), and the individual organic phases were concentrated in vacuo to obtain extracts. Analytical samples prepared from each extract (5 mg/mL in MeOH) were subjected to HPLC-DAD-ESI(±)MS analysis (Agilent Zorbax SB-C_8 column, 150 × 4.6 mm, 5 μm, 1 mL/min gradient elution from 90% H_2O/MeCN to 100% MeCN over 15 min with an isocratic 0.05% formic acid modifier; column temperature 30 °C; UV 210 and 254 nm; 5 μL injection). All cultivation, extraction, and analysis experiments were performed in triplicate.

Analysis of Liquid-Phase Biotransformation of Tetracyclines 3 and 6. Liquid-phase cultivation media were prepared using PYG broth (60 mL of 2% glucose, 1% peptone, 0.5% yeast extract in sterile water) in 250 mL Schott flasks. Each flask was treated with 0.5 mg/mL of the HCl salt of **3** or **6**, followed by inoculating in situ with 5 d seed cultures (600 μL) of 13 strains. The inoculated broths, together with negative control broths lacking treatment with **3** and **6**, were subjected to static incubation in the dark at 26.5 °C for 15 and 30 d, after which they were extracted with EtOAc (2 × 60 mL), and the individual organic phases were concentrated in vacuo to obtain extracts. Analytical samples prepared from each extract (5 mg/mL in MeOH) were subjected to HPLC-DAD-ESI(±)MS analysis with the identical elution condition for solid-phase biotransformation study. All cultivation, extract, and analysis experiments were performed in triplicate.

Preparative-Scale Biotransformation of Tetracyclines 3−7. Solid-phase cultivation media were prepared using PYG agar and treated with the HCl salts of **3**−**7** (40 mg each, prepared in 200 μL sterile H_2O), respectively. An individual agar plate inoculated (streaked) with *Paecilomyces* sp. (CMB-MF010) was sealed with parafilm to prevent dehydration. These plates, including substrate control plates without fungal inoculation, were incubated at 26.5 °C for two different time periods, 15 and 30 d, after which they were extracted with EtOAc (2 × 50 mL), and the individual organic phases were concentrated *in vacuo* to obtain extracts.

Isolation of Tetracycline (3) Biotransformation Products. The EtOAc extract (29.6 mg) of a 30 d PYG agar plate cultivation of *Paecilomyces* sp. (CMB-MF010) in the presence of the HCl salt of **3** (40 mg) was fractionated by HPLC (Agilent Zorbax SB-C_3 column, 250 × 9.4 mm, 5 μm, 3 mL/min gradient elution from 70% to 50% H_2O/MeCN over 15 min followed by a 5 min hold at 100% MeCN, with an isocratic 0.01% TFA modifier) to afford *seco*-cycline A (**9**) (t_R = 9.7 min; 8.8 mg, 21.9%), *seco*-cycline B (**10**) (t_R = 10.3 min; 4.0 mg, 13.5%), and *seco*-cycline C (**11**) (t_R = 13.8 min; 3.0 mg, 10.1%). The EtOAc extract (26.2 mg) of a 15 d PYG agar plate cultivation of *Paecilomyces* sp. (CMB-MF010) in the presence of the HCl salt of tetracycline (**3**) (40 mg) was fractionated by HPLC (Phenomenex Luna C_8 column, 250 × 21.2 mm, 10 μm, 20 mL/min gradient elution from 70% H_2O/MeCN to MeCN over 20 min, with an isocratic 0.01% TFA modifier) to yield *seco*-cycline D (**12**) (t_R = 9.7 min; 1.7 mg, 6.5%).

Isolation of Minocycline (4) Biotransformation Products. The EtOAc extract (7.5 mg) of a 30 d PYG agar plate cultivation of *Paecilomyces* sp. (CMB-MF010) in the presence of the HCl salt of **4** (40 mg) was fractionated by HPLC (Phenomenex Luna C_{18} column, 250 × 21.2 mm, 10 μm, 20 mL/min gradient elution from 80% to 65% H_2O/MeCN over 20 min, with an isocratic 0.01% TFA modifier) to yield *seco*-cycline E (**13**) (t_R = 7.7 min; 1.7 mg, 22.7%) and *seco*-cycline F (**14**) (t_R = 8.3 min; 1.9 mg, 25.3%).

Isolation of Chlortetracycline (5) Biotransformation Products. Although low yields from the *Paecilomyces* sp. (CMB-MF010) biotransformation of the HCl salt of **5** precluded spectroscopic characterization of products, the *seco*-cyclines A (**9**) and B (**10**) could be identified based on comparison with authentic samples. The putative 7-chlorinated analogues, *seco*-cyclines G (**18**) and H (**19**), were purified as a mixture (t_R = 12.3 min; 0.4 mg, 3.0%) using HPLC (Phenomenex Luna C_8 column, 250 × 21.2 mm, 10 μm, 20 mL/min gradient elution from 80% to 15% H_2O/MeCN over 20 min, with an isocratic 0.01% TFA modifier) and tentatively identified on the basis of UV−vis and HRESIMS analysis and mechanistic considerations (Figure 11).

Isolation of Oxytetracycline (6) Biotransformation Products. The EtOAc extract (18.3 mg) of a 30 d PYG agar plate cultivation of *Paecilomyces* sp. (CMB-MF010) in the presence of the HCl salt of **6** (40 mg) was fractionated by HPLC (Phenomenex Luna C_8 column,

DOI: 10.1021/acs.joc.6b01272
J. Org. Chem. 2016, 81, 6186−6194

250 × 21.2 mm, 10 μm, 20 mL/min gradient elution from 75% to 10% H_2O/MeCN over 20 min, with an isocratic 0.01% TFA modifier) to yield *hemi*-cycline A (**20**) (t_R = 7.2 min; 4.0 mg, 21.9%) and *hemi*-cycline B (**21**) (t_R = 10.4 min; 0.3 mg, 1.6%).

Isolation of Doxycycline (7) Biotransformation Products. The EtOAc extract (15.3 mg) of a 30 d PYG agar plate cultivation of *Paecilomyces* sp. (CMB-MF010) in the presence of the HCl salt of **7** (40 mg) was fractionated by HPLC (Phenomenex Luna C_{18} column, 250 × 21.2 mm, 10 μm, 20 mL/min gradient elution from 85% to 10% H_2O/MeCN over 20 min, with an isocratic 0.01% TFA modifier) to yield *hemi*-cycline C (**22**) (t_R = 12.5 min; 0.3 mg, 2.0%), *hemi*-cycline D (**23**) (t_R = 12.7 min; 1.9 mg, 12.4%), and *hemi*-cycline E (**24**) (t_R = 9.6 min; 0.4 mg, 2.6%).

Characterization of Biotransformation Products 9−14 and 18−24. *seco-Cycline A (9):* yellow amorphous powder; NMR (600 MHz, DMSO-d_6) see Table S7; ESI(+)MS *m/z* 370 $[M - H_2O + H]^+$, 410 $[M + Na]^+$, ESI(−)MS *m/z* 386 $[M - H]^-$; HRESI(+)MS *m/z* 410.0847 $[M + Na]^+$ (calcd for $C_{19}H_{17}NO_8Na$, 410.0846).

seco-Cycline B (10): red crystals; $[\alpha]_D^{22}$ −154.2 (*c* 0.08, MeOH); UV (MeOH) λ_{max} (log ε) 261 (4.23), 317 (4.16) nm; NMR (600 MHz, DMSO-d_6) see Table S8; ESI(+)MS *m/z* 369 $[M - H_2O + H]^+$, 409 $[M + Na]^+$, ESI(−)MS *m/z* 385 $[M - H]^-$; HRESI(+)MS *m/z* 409.1008 $[M + Na]^+$ (calcd for $C_{19}H_{18}N_2O_7Na$, 409.1006).

seco-Cycline C (11): yellow amorphous powder; $[\alpha]_D^{22}$ −470.7 (*c* 0.14, MeOH); UV (MeOH) λ_{max} (log ε) 261 (4.28), 295 (4.14) nm; NMR (600 MHz, DMSO-d_6) see Table S9; ESI(+)MS *m/z* 370 $[M + H]^+$, 408 $[M + K]^+$, ESI(−)MS *m/z* 368 $[M - H]^-$; HRESI(+)MS *m/z* 392.0735 $[M + Na]^+$ (calcd for $C_{19}H_{15}NO_7Na$, 392.0741).

seco-Cycline D (12):[9,10] dark orange powder; $[\alpha]_D^{22}$ −93.9 (*c* 0.05, MeOH); UV (MeOH) λ_{max} (log ε) 272 (4.27), 300 (4.35) nm; NMR (600 MHz, DMSO-d_6) see Table S10; ESI(+)MS *m/z* 396 $[M - H_2O + H]^+$, 431 $[M + NH_4]^+$, ESI(−)MS *m/z* 412 $[M - H]^-$; HRESI(+)MS *m/z* 436.0632 $[M + Na]^+$ (calcd for $C_{20}H_{15}NO_9Na$, 436.0639).

seco-Cycline E (13):[11] dark orange powder; $[\alpha]_D^{22}$ −13.4 (*c* 0.10, MeOH); UV (MeOH) λ_{max} (log ε) 244 (4.14), 261 (4.11), 300 (4.14), 365 (3.33) nm; NMR (600 MHz, DMSO-d_6) see Table S11; ESI(+)MS *m/z* 401 $[M + H]^+$, ESI(−)MS *m/z* 399 $[M - H]^-$; HRESI(+)MS *m/z* 401.1347 $[M + H]^+$ (calcd for $C_{20}H_{21}N_2O_7$, 401.1343).

seco-Cycline F (14): red amorphous powder; $[\alpha]_D^{22}$ −9.1 (*c* 0.10, MeOH); UV (MeOH) λ_{max} (log ε) 247 (4.17), 266 (4.19), 317 (4.17), 324 (4.17) nm; NMR (600 MHz, DMSO-d_6) see Table S12; ESI(+)MS *m/z* 400 $[M + H]^+$, ESI(−)MS *m/z* 398 $[M - H]^-$; HRESI(+)MS *m/z* 400.1507 $[M + H]^+$ (calcd for $C_{20}H_{22}N_3O_6$, 400.1503).

seco-Cycline G (18): yellow amorphous powder; UV (MeCN/H_2O with 0.05 formic acid); λ_{max} 224, 276 nm (from HPLC-DAD); ESI(+)MS *m/z* 444 $[M + Na]^+$, ESI(−)MS *m/z* 420 $[M - H]^-$; HRESI(−)MS *m/z* 420.0491 $[M - H]^-$ (calcd for $C_{19}H_{15}ClNO_8$, 420.0492).

seco-Cycline H (19): orange amorphous powder; UV (MeCN/H_2O with 0.05 formic acid); λ_{max} 262, 308 nm (from HPLC-DAD); ESI(+)MS *m/z* 443 $[M + Na]^+$, ESI(−)MS *m/z* 419 $[M - H]^-$; HRESI(−)MS *m/z* 419.0651 $[M - H]^-$ (calcd for $C_{19}H_{16}ClN_2O_7$, 419.0652).

hemi-Cycline A (20): pale yellow oil; $[\alpha]_D^{22}$ +17.0 (*c* 0.15, MeOH); UV (MeOH) λ_{max} (log ε) 261 (3.91), 335 (3.57) nm; NMR (600 MHz, CD_3OD) see Table S13; ESI(+)MS *m/z* 205 $[M - H_2O + H]^+$, 223 $[M + H]^+$, ESI(−)MS *m/z* 221 $[M - H]^-$; HRESI(−)MS *m/z* 221.0824 $[M - H]^-$ (calcd for $C_{12}H_{13}O_4$, 221.0819).

hemi-Cycline B (21): pale yellow oil; UV (MeOH) λ_{max} (log ε) 261 (3.94), 335 (3.59) nm; NMR (600 MHz, CD_3OD) see Table S14; ESI(+)MS *m/z* 187 $[M - H_2O - OAc]^+$, 287 $[M + Na]^+$; HRESI(+)MS *m/z* 287.0889 $[M + Na]^+$ (calcd for $C_{14}H_{16}O_5Na$, 287.0890).

hemi-Cycline C (22): colorless oil; UV (MeOH) λ_{max} (log ε) 261 (3.85), 331 (3.48) nm; NMR (600 MHz, CD_3OD) see Table S15; ESI(+)MS *m/z* 207 $[M + H]^+$, ESI(−)MS *m/z* 205 $[M - H]^-$; HRESI(+)MS *m/z* 229.0840 $[M + Na]^+$ (calcd for $C_{12}H_{14}O_3Na$, 229.0835).

hemi-Cycline D (23). Colorless oil; $[\alpha]_D^{22}$ − 19.0 (*c* 0.10, MeOH); UV (MeOH) λ_{max} (log ε) 261 (4.00), 333 (3.63) nm; NMR (600 MHz, CD_3OD) see Table S16; ESI(+)MS *m/z* 221 $[M + H]^+$, 243 $[M + Na]^+$, ESI(−)MS *m/z* 219 $[M - H]^-$; HRESI(+)MS *m/z* 243.0635 $[M + Na]^+$ (calcd for $C_{12}H_{12}O_4Na$, 243.0628).

hemi-Cycline E (24). Colorless oil; UV (MeOH) λ_{max} (log ε) 270 (4.02), 357 (3.53) nm; NMR (600 MHz, CD_3OD) see Table S17; ESI(+)MS *m/z* 237 $[M + H]^+$, 259 $[M + Na]^+$, ESI(−)MS *m/z* 235 $[M - H]^-$; HRESI(+)MS *m/z* 259.0573 $[M + Na]^+$ (calcd for $C_{12}H_{12}O_5Na$, 259.0577).

X-ray Crystallographic Analysis of 10·H_2O. A single crystal of **10**·H_2O was obtained from MeOH by slow evaporation at room temperature. Data were collected at 190 K using an Oxford Diffraction Gemini CCD diffractometer with Cu Kα radiation, and the crystal was cooled with an Oxford Cryosystems Desktop Cooler. Data reduction was performed with the CrysAllisPro program (Oxford Diffraction vers. 171.34.40). The structure was solved by direct methods with SHELXS86 and refined with SHELX97.[19] The thermal ellipsoid diagram was produced with ORTEP3,[20] and all calculations were performed within the WinGX package.[21] Data: $C_{19}H_{18}N_2O_7.H_2O$, *M* = 404.37, monoclinic, *a* = 8.1814(3) Å, *b* = 6.3315(3) Å, *c* = 16.7915(11) Å, *V* = 868.85(8) Å^3, *T* = 190(2) K, space group $P2_1$, *Z* = 2, 4657 reflections measured, 1848 unique (R_{int} = 0.0340) which were used in all calculations. The final *R*(obsd data) was 0.0412, goodness of fit 1.148. CCDC no. 1480142. The absolute configuration of **10** was confirmed by the methodology of Hooft et al.[22]

■ ASSOCIATED CONTENT

Ⓢ Supporting Information

The Supporting Information is available free of charge on the ACS Publications website at DOI: 10.1021/acs.joc.6b01272.

^{1}H and ^{13}C NMR spectra and tabulated 1D and 2D NMR data of the tetracyclines **3**−**7**, *seco*-cyclines A−F (**9**−**14**), and *hemi*-cyclines A−E (**20**−**24**), HPLC chromatograms of biotransformation studies, bioassay methodology and results, and X-ray crystallography data (PDF)

X-ray crystallographic data for **10** (CIF)

■ AUTHOR INFORMATION

Corresponding Author

*E-mail: r.capon@uq.edu.au.

Notes

The authors declare no competing financial interest.

■ ACKNOWLEDGMENTS

This research was funded in part by the Institute for Molecular Bioscience, UQ, and the Australian Research Council (DP120100183). Z.S. acknowledges UQ for an International Postgraduate Research Scholarship. We thank M. Quezada (UQ) for bioassay support, E. Lacey (BioAustralis) for a gift of chlortetracycline, minocycline, and doxycycline, and D. Paterson and H. Zowawi (UQCCR) for multidrug-resistant bacteria isolates.

■ REFERENCES

(1) Shang, Z.; Salim, A. A.; Khalil, Z.; Quezada, M.; Bernhardt, P. V.; Capon, R. J. *J. Org. Chem.* **2015**, *80*, 12501−12508.

(2) Nicolaou, K. C.; Nilewski, C.; Hale, C. R.; Ioannidou, H. A.; ElMarrouni, A.; Koch, L. G. *Angew. Chem., Int. Ed.* **2013**, *52*, 8736−8741.

DOI: 10.1021/acs.joc.6b01272
J. Org. Chem. 2016, 81, 6186−6194

(3) Nicolaou, K. C.; Hale, C. R.; Nilewski, C.; Ioannidou, H. A.; ElMarrouni, A.; Nilewski, L. G.; Beabout, K.; Wang, T. T.; Shamoo, Y. *J. Am. Chem. Soc.* **2014**, *136*, 12137−12160.
(4) Valcavi, U.; Brandt, A.; Corsi, G. B.; Minoja, F.; Pascucci, G. *J. Antibiot.* **1981**, *34*, 34−39.
(5) Cvančarová, M.; Moeder, M.; Filipová, A.; Reemtsma, T.; Cajthaml, T. *Environ. Sci. Technol.* **2013**, *47*, 14128−14136.
(6) Rusch, M.; Kauschat, A.; Spielmeyer, A.; Römpp, A.; Hausmann, H.; Zorn, H.; Hamscher, G. *J. Agric. Food Chem.* **2015**, *63*, 6897−6904.
(7) Prieto, A.; Möder, M.; Rodil, R.; Adrian, L.; Marco-Urrea, E. *Bioresour. Technol.* **2011**, *102*, 10987−10995.
(8) McCormick, J. R. D.; Fox, S. M.; Smith, L. L.; Bitler, B. A.; Reichenthal, J.; Origoni, V. E.; Muller, W. H.; Winterbottom, R.; Doerschuk, A. P. *J. Am. Chem. Soc.* **1957**, *79*, 2849−2858.
(9) Kinney, R. W.; Neidleman, S. L.; Weisenborn, F. L.; Schwarz, J. S. P. US 3462487 A, 1969.
(10) Schwarz, J. S. P.; Weisenborn, F. L.; Neidleman, S. L.; Kinney, R. W. US 3438999 A, 1969.
(11) Gu, J.; Cai, P.; Gong, Y.; Ruppen, M. E.; Storz, T. *J. Antibiot.* **2010**, *63*, 693−698.
(12) Søeborg, T.; Ingerslev, F.; Halling-Sørensen, B. *Chemosphere* **2004**, *57*, 1515−1524.
(13) Arikan, O. A. *J. Hazard. Mater.* **2008**, *158*, 485−490.
(14) Deseo, M. A.; Hunter, l. S.; Waterman, P. G. *J. Antibiot.* **2005**, *58*, 822−827.
(15) Chopra, I.; Roberts, M. *Microbiol. Mol. Biol. Rev.* **2001**, *65*, 232−260.
(16) Lipsitch, M.; Singer, R. S.; Levin, B. R. *Proc. Natl. Acad. Sci. U. S. A.* **2002**, *99*, 5752−5754.
(17) Kümmerer, K. *Chemosphere* **2009**, *75*, 417−434.
(18) Baquero, F.; Martínez, J. L.; Cantón, R. *Curr. Opin. Biotechnol.* **2008**, *19*, 260−265.
(19) Sheldrick, G. M. *Acta Crystallogr., Sect. A: Found. Crystallogr.* **2008**, *64*, 112−122.
(20) Farrugia, L. J. *J. Appl. Crystallogr.* **1997**, *30*, 565.
(21) Farrugia, L. J. *J. Appl. Crystallogr.* **1999**, *32*, 837−838.
(22) Hooft, R. W.; Straver, L. H.; Spek, A. L. *J. Appl. Crystallogr.* **2008**, *41*, 96−103.

DOI: 10.1021/acs.joc.6b01272
J. Org. Chem. 2016, 81, 6186−6194